Journal of Asian Earth Sciences 129 (2016) 67–80

Contents lists available at ScienceDirect

Journal of Asian Earth Sciences

journal homepage: www.elsevier.com/locate/jseaes

Full length article

Re-Os isotopic and trace element compositions of pyrite and origin of the Cretaceous Jinchang porphyry Cu-Au deposit, Heilongjiang Province, NE China

Peng Zhang [a], Xiao-Wen Huang [b,*], Bin Cui [a], Bo-Chao Wang [c], Yi-Fan Yin [b], Jing-Rui Wang [d]

[a] School of Earth Sciences and Resources, China University of Geosciences, Beijing 10083, China
[b] State Key Laboratory of Ore Deposit Geochemistry, Institute of Geochemistry, Chinese Academy of Sciences, Guiyang 550081, China
[c] No. 3 Party of Gold Geology, CAPF, Haerbin 150086, China
[d] No. 1 Party of Gold Geology, CAPF, Mudanjiang 157000, China

ARTICLE INFO

Article history:
Received 3 November 2015
Received in revised form 29 July 2016
Accepted 29 July 2016
Available online 30 July 2016

Keywords:
Pyrite
Re-Os isotopes
In situ trace elements
Fluid evolution
Porphyry Cu-Au
NE China

ABSTRACT

The Jinchang Cu-Au deposit in Northeast China contains more than 76 tons of Au and 4683 tons of Cu with average ore grades of 11.34 g/t Au and 1.44% Cu. The deposit is typical of porphyry types and consists of gold orebodies mainly hosted in a ~113 Ma granitic porphyry and breccia pipes within the porphyry intrusion. Mineralization is closely associated with early potassic alteration and late phyllic alteration. Pyrite is the main Au-bearing mineral and contains 1.48–18.9 ppb Re and 11.4–38 ppt common Os. Extremely low common Os concentrations and high Re/Os ratios are indicative of derivation of ore-forming materials from the crust. Low Re in pyrite from the Jinchang deposit may indicate a mixing source of mantle and crust or a crustal source. Five Re-Os isotopic analyses yield a model 1 isochron age of 114 ± 22 Ma (2σ, MSWD = 0.15), similar to the age of the host porphyry. Pyrite contains detectable Co, Ni, Cu, Zn, As, Ag, Au, Sb, Pb and Bi. Pyrite has Co/Ni ratios similar to that of volcanogenic and hydrothermal sulfide deposits, indicating a magmatic-hydrothermal origin, and has Au and As contents similar to that of porphyry-epithermal systems. Pyrite grains from potassic and phyllic alteration stages have different trace element contents, reflecting the evolution of ore-forming fluids from magmatic dominated to magmatic mixed with meteoric water. In combination with regional geology, our new results are suggestive of origin of the Jinchang Cu-Au deposit from contemporary intrusions of granitic porphyries related to the Early Cretaceous subduction of the Paleo-Pacific plate.

1. Introduction

In NE China, complex tectono-magmatic events in Mesozoic produced numerous large-scale mineral deposits (Chen et al., 1998, 2008, 2009; Xiao et al., 2003, 2008; Goldfarb et al., 2014; Mao et al., 2014; Zeng et al., 2015; Wu et al., 2016). The Mesozoic metallogenic province in NE China, as part of the western Circum-Pacific metallogenic belt, was considered to be closely related to the subduction of the Paleo-Pacific plate (Mao et al., 2014 and references therein). Both porphyry Cu-Mo (Au) and porphyry Mo deposits are common in NE China, and are mainly distributed along the margin of the North China Craton (NCC) and Central Asian Orogenic Belt (CAOB) (Fig. 1a). There are two types of porphyry Cu systems, i.e. porphyry skarn Cu system mainly in inland with ages of 175–135 Ma and porphyry Cu-Au and epithermal Au system at the continental margin with ages of ca. 100 Ma (Fig. 1a). The Jinchang Cu-Au deposit in Heilongjiang province and Xiaoxinancha Cu-Au deposit in Jilin province are both typical of porphyry deposits in NE China (Fig. 1a). The Jinchang deposit is particularly important with more than 76 tons of Au and has become a giant Au deposit in China (Zhou et al., 2002; Goldfarb et al., 2014). In spite of its economic importance, the ore genesis of the Jinchang deposit remains controversial and thus its relation to regional tectonic and magmatic activities is not well constrained.

Two fundamental problems regarding the genesis of porphyry Cu-Au deposits are the source of the metals and the timing of hydrothermal activities. Many fluid inclusion studies concerned the source and composition of ore-forming fluids and thought that the Jinchang deposit is epithermal and formed from low temperature fluids with low concentrations of CO_2 in auriferous quartz-sulfide veins (Zhu et al., 2003). Other views include porphyry-related origin of the deposit that formed from high

* Corresponding author.
E-mail address: huangxiaowen@vip.gyig.ac.cn (X.-W. Huang).

http://dx.doi.org/10.1016/j.jseaes.2016.07.032
1367-9120/

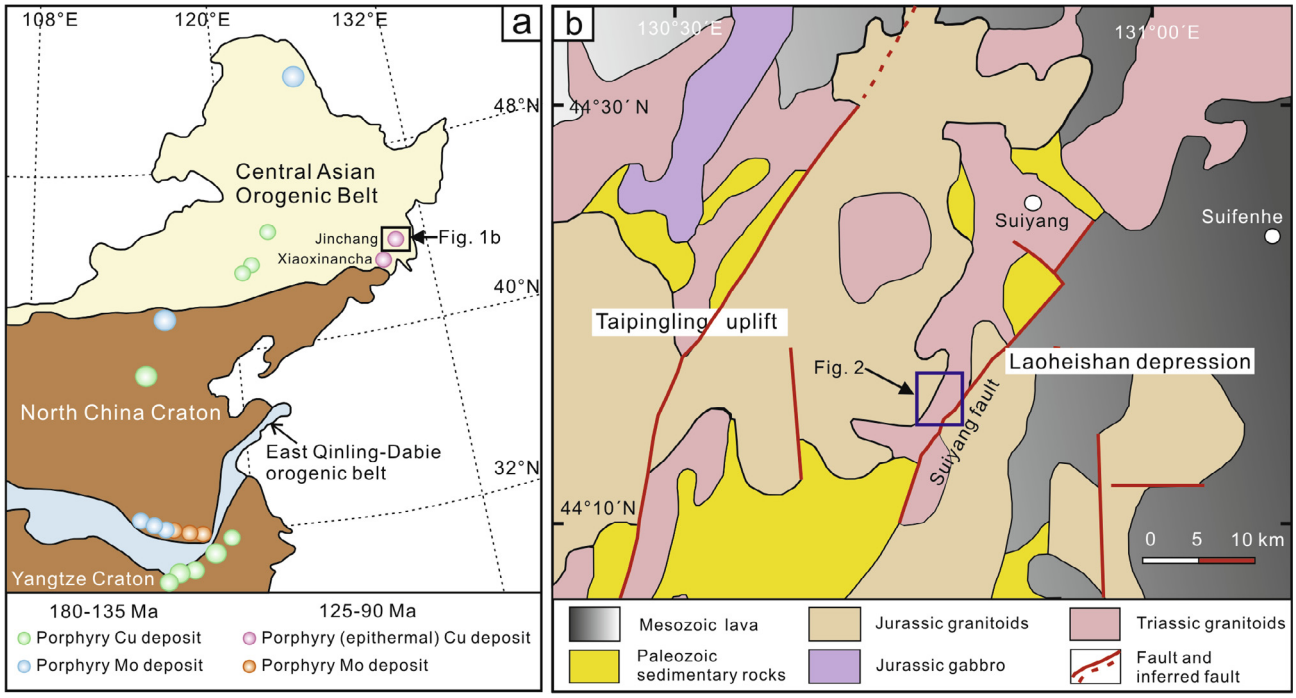

Fig. 1. (a) Distribution of major porphyry copper and molybdenum deposits in East China and the location of the Jinchang area (modified from Mao et al., 2014); (b) regional geological map of the Jinchang Cu-Au deposit (after Zhang et al., 2014).

temperature fluids with high salinities (30–60% NaCl) (Jia et al., 2008). Overprinting of a porphyry-epithermal type deposit was also proposed (Wang et al., 2007). Zhang et al. (2008) proposed that it is an orogenic gold deposit formed from CO_2-rich fluids in breccias, whereas Zhang et al. (2014) considered that it is oxidized intrusion-related deposit formed from high temperature (200–480 °C) fluids.

Debate about the origin is also due to the lack of the direct mineralization age. Ar-Ar and Rb-Sr dating methods were used to constrain the timing of gold mineralization. For example, Ar-Ar dating of quartz from auriferous quartz-sulfide veins and Rb-Sr dating of sericite from the gold-mineralized phyllic-altered granodiorite and granite porphyry yielded ages of ca. 107–122 Ma (Jia et al., 2008; Qing et al., 2012; Zhang et al., 2013). However, dating of ore minerals from this deposit is not available using these traditional dating methods.

Over the past few decades, the Re-Os isotope system has been used to date ore deposits. Sulfide minerals, pyrite, arsenopyrite, and chalcopyrite, have low Re and Os concentrations and have been used successfully for Re-Os dating of hydrothermal ore deposits (e.g., Stein et al., 1998, 2000; Mathur et al., 1999; Morelli et al., 2004; Selby et al., 2009; Huang et al., 2013a–c). Previous studies have shown that the Re-Os isotope system of auriferous pyrite can be a good method to date Au and Cu-Au deposits (e.g., Frei et al., 1998; Arne et al., 2001; Kirk et al., 2001; Cardon et al., 2008; Kerr and Selby, 2012; Lawley et al., 2013).

Pyrite is the main gold-bearing mineral of Cu-Au deposits and hosts numerous minor and trace elements. Most of trace elements in pyrite are at low concentration levels, but can provide useful information about ore-forming processes. In recent years, in situ LA-ICP-MS technique has been widely used to determine trace element contents of pyrite in the studies of hydrothermal deposits (e.g., Cook et al., 2009; Large et al., 2009; Koglin et al., 2010; Maydagán et al., 2013; Reich et al., 2013; Cioacă et al., 2014; Deditius et al., 2014; Makoundi et al., 2014).

In this study, we present reliable Re-Os isotopic data of auriferous pyrite from the Jinchang Cu-Au deposit, in order to constrain the timing of gold mineralization. In situ trace elemental compositions of the auriferous pyrite are also reported and are used in combination with the new Re-Os isotopic data to discuss the possible sources of metals in the ore-forming fluids. With the new dataset, we further discuss the regional implications for gold metallogeny in relation to the subduction of the Paleo-Pacific plate.

2. Geological background

2.1. Regional geology

The area across the northern NCC and the Central Asian Orogenic Belt and belongs to the western Circum-Pacific tectonic regime (Fig. 1a). The entire area has a long tectono-magmatic history, including the formation of Archean-Paleoproterozoic lithotectonic units, Middle-Late Proterozoic rifting, subduction-collision related to the closure of the Paleo-Asian Ocean, and Mesozoic intracontinental tectono-thermal events (Sengör et al., 1993; Xiao et al., 2003; Yang et al., 2003; Pirajno et al., 2009; Safonova, 2009). During the Paleozoic, the geodynamic evolution of the Paleo-Asian Ocean is largely responsible for the tectonic framework of NE China, which is characterized by several convergent orogenic boundaries (Windley et al., 2002; Xiao et al., 2003). During the Mesozoic, this area is dominated by intracontinental orogenesis that was later overprinted by the westward subduction of the Paleo-Pacific plate (Pirajno et al., 2009). This tectonic transition from Indosinian to Yanshanian tectono-thermal events was related to the Paleo-Pacific subduction and is responsible for intense mantle-crust interaction and melting of the lower crust, resulting in a large-scale mineralization in the northern NCC and eastern part of CAOB (Chen et al., 1998; Zhai et al., 2003).

In the Jinchang area, the junction of the Laoheishan Depression and Taipingling Uplift of NE China (Zhang et al., 2013) (Fig. 1b), the NNE trending transcurrent Suiyang fault controls the distribution of subsidiary faults (Fig. 1b). Abundant Mesozoic granitic intrusions and minor Mesozoic–Cenozoic volcano–sedimentary

successions are mainly spread in the Taipingling Uplift (Jia et al., 2004; Zhang et al., 2008; Liu et al., 2010). Granitoids in this uplift include granodiorite, monzogranite, syenogranite and alkali-feldspar granite, but there are also minor diorite and gabbro (Fig. 1b). They are mostly dated at ~200 Ma (Wu et al., 2011; Zhang et al., 2013; Zhou and Wilde, 2013). Triassic volcano–sedimentary rocks in the Laoheishan Depression have zircon with U–Pb ages of ca. 200–220 Ma (Fig. 1b) (Xu et al., 2009).

2.2. Deposit geology

Mesozoic granitoids are dominant in the Jinchang area, surrounded by minor Jurassic volcano-sedimentary rocks and mafic to felsic dikes (Fig. 2). The granitoids include granodiorite, diorite, granite porphyry, and monzogranite. The granitoids in this area contain zircons with U-Pb ages of ca. 200 Ma (Zhang, 2007; Men et al., 2008; Lu et al., 2009; Zhang et al., 2013; Zhao, 2013), whereas mafic to felsic dikes mainly emplaced at ca. 110 Ma (Lu et al., 2009; Qian et al., 2012; Zhao et al., 2012; Zhang et al., 2013; Zhao, 2013) (Fig. 2). The volcano-sedimentary rocks have U-Pb ages of 200–220 Ma (Xu et al., 2009). The major ore-hosting structures are breccia pipes.

The Jinchang deposit was discovered and explored since 1990s (Mu et al., 2000; Chen et al., 2002). More than 76 tons of Au and 4683 tons of Cu have been mined (unpublished data from No. 1 Party of Gold Geology, Mudanjiang of China). Orebodies in the Jinchang deposit are hosted in breccia pipes and are controlled by faults (Fig. 2). Breccia pipes occur mainly in EW-trending faults, at the intersection of two sets of faults striking in different directions. There are more than 20 orebodies in the Jinchang deposit, among which the largest J1 orebody is a breccia pipe orebody, 60 m in length, 45 m in width, and >500 m in depth. The average gold grade is 8.1 g/t (Zhao, 2013). There are three types of ores, breccia, quartz-sulfide vein and stockwork types, accounting for 44%, 36%, and 20% of the total gold production, respectively. The breccia type ores occur in the breccia pipes and contain large amounts of rock breccias (Fig. 3a), which have the gold grade ranging from 8 to 88 g/t (Zhao, 2013). The size of the angular breccia fragments ranges widely from centimeters to a few meters. Fragments of breccia in the ores are mainly granite and granite porphyry composed of quartz, K-feldspar and plagioclase (Fig. 3b–d). Matrices of breccia ores are mainly gold-bearing quartz-sulfide veins or auriferous pyrite veins, hydrothermal alteration minerals, sericite, epidote, kaolinite and chlorite, and minor granite. The quartz-sulfide vein type ores mainly occur in the fractures controlled by the radial and linear faults (Fig. 3e) with variable gold grade of 1.5–18.6 g/t (Zhao, 2013). The stockwork type ores occur as veins in hydrothermally altered granitic wall rocks at the depth of the breccia pipes and are characterized by quartz-sulfide stockworks or veinlets (Fig. 3f), with an average gold grade of 5.31 g/t (Zhao, 2013). Mineral assemblages are similar for different types of ores. Sulfide minerals are mainly pyrite, chalcopyrite, galena, and sphalerite (Fig. 3g and h). Native gold is locally present (Fig. 3i). Gangue minerals are quartz, sericite, feldspar, epidote, kaolinite, biotite, chlorite and calcite.

Two alteration stages, early potassic and late phyllic alteration stages, can be indentified in the J1 orebody of the Jinchang deposit. Potassic alteration at the −20 m and 30 m levels has a mineral assemblage of K-feldspar, quartz, pyrite, chalcopyrite and native gold (Fig. 3c, f, h and i). Auriferous pyrite veins and quartz-pyrite-chalcopyrite veins are extensive in the potassic stage. The potassic alteration is overprinted by other types of alterations, similar to porphyry deposit systems elsewhere (e.g., Maydagán et al., 2013). Phyllic alteration occurs at the 80 m level, characterized

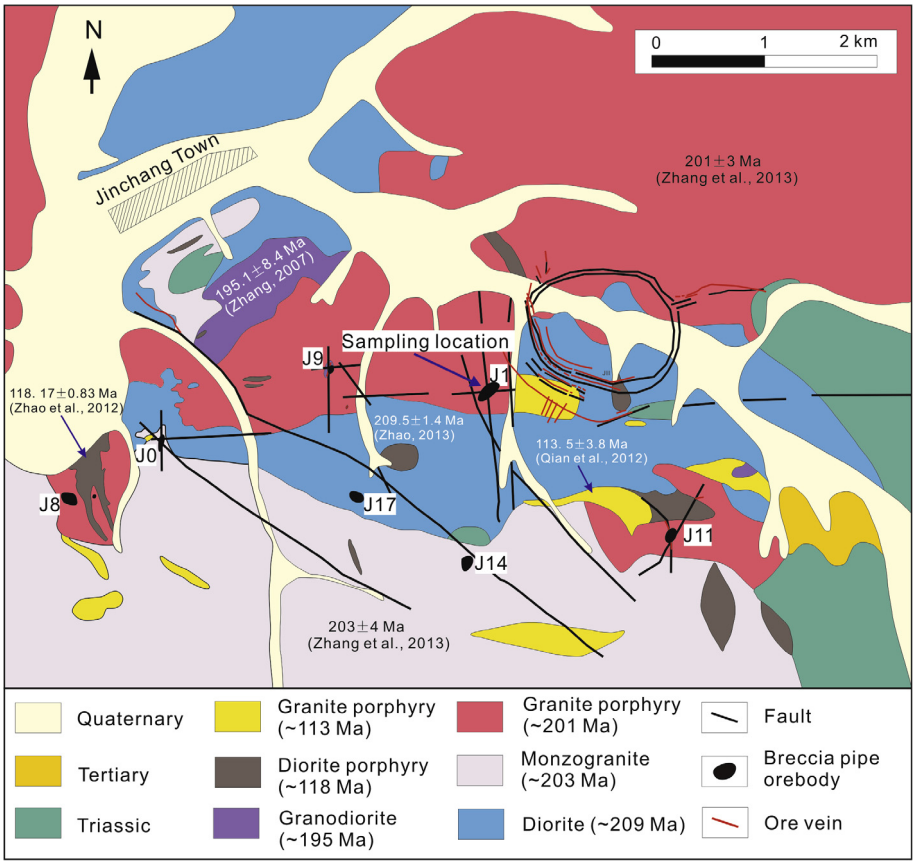

Fig. 2. Local geological map of the Jinchang Cu-Au deposit (after Zhao et al., 2012; Zhang et al., 2014). Ages indicated in this figure are zircon U-Pb ages.

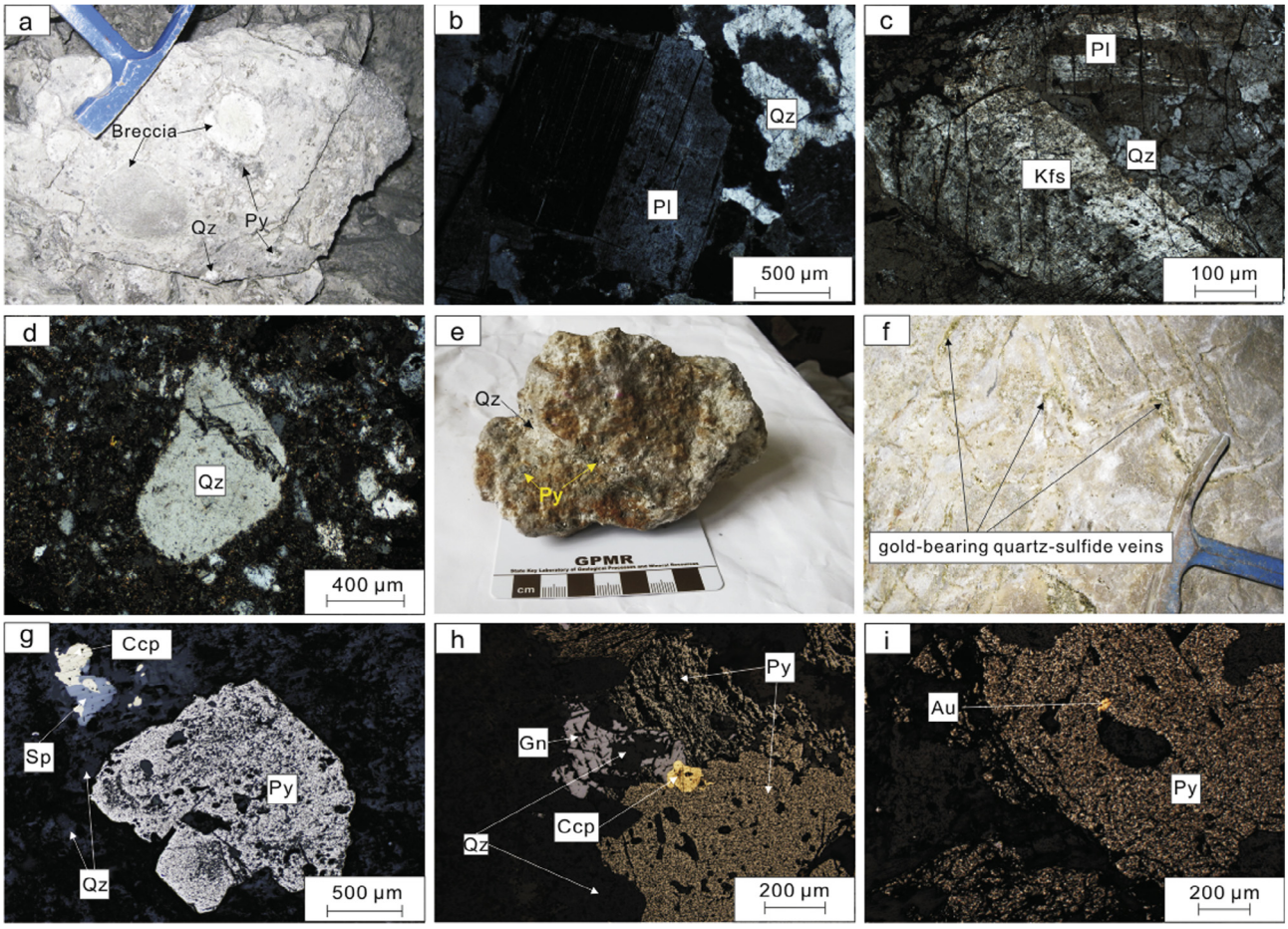

Fig. 3. Field photos and photomicrographs of ores from the J1 orebody of the Jinchang Cu-Au deposit. (a) Breccia type ore from breccia pipe of the J1 orebody composed of rock breccias and pyrite; (b) rock breccia consisting of plagioclase phenocryst and quartz; (c) altered rock breccia composed of plagioclase phenocryst, K-feldspar phenocryst and quartz; (d) quartz phenocryst from altered breccia; (e) quartz-sulfide vein type ore mainly composed of quartz and pyrite; (f) quartz-sulfide veins in altered granite porphyry from −20 m level of the J1 orebody; (g) ore composed of pyrite, chalcopyrite, sphalerite, and quartz; (h) ore composed of pyrite, chalcopyrite, galena, and quartz; (i) native gold in pyrite. Abbreviation: Qz, quartz; Pl, plagioclase; Kfs, K-feldspar; Py, pyrite; Ccp, chalcopyrite; Sp, sphalerite; Gn, galena; Au, gold.

by a mineral assemblage of quartz, sericite, pyrite, chalcopyrite, sphalerite and minor galena (Fig. 3a, b and g). Gold-bearing quartz-sulfide veins are dominant in the phyllic stage.

3. Sampling and analytical methods

Samples in this study were taken from 3 mining sections (80 m, 30 m and −20 m level) of the J1 orebody in the Jinchang Cu-Au deposit. Samples for Re-Os isotope analyses are taken from ores with potassic alteration, whereas those for trace element analyses are from ores with both alteration types.

3.1. Re-Os isotopes

Pyrite separates are from the gold-bearing quartz-sulfide veins and auriferous pyrite veins in the matrices of breccias or the granite porphyry. Pyrite grains were separated by heavy liquid and were then hand-picked under a binocular microscope. Pyrite grains range in size from ~180 to 250 μm.

Re and Os isotopes were analyzed using a PE ELAN DRC-e ICP-MS in the State Key Laboratory of Ore Deposit Geochemistry, Institute of Geochemistry, Chinese Academy of Sciences (IGCAS), Guiyang, China. The detailed analytical procedure was described in Qi et al. (2013) and Huang et al. (2015). Approximately 0.5–1 g of pyrite were weighed and loaded into a 200 ml Carius tube with known amounts of ^{185}Re and ^{190}Os spikes. For samples more than 1.5 g, they were firstly digested using auto-made device to remove sulfur (Qi et al., 2010). Samples were then digested and equilibrated using 10–20 ml concentrated HNO_3 and 2 ml HCl at 200 °C for about 12 h. Osmium was separated as OsO_4 from the matrix using the in situ distillation equipment, whereas Re was separated from the remaining solution after Os distillation using the anion exchange resin (Biorad AG 1 × 8, 200–400 mesh) (Qi et al., 2007, 2010). Iridium was added to Re-bearing and Os-bearing solutions for mass discrimination correction. The calibration method was referred to Schoenberg et al. (2000). Procedural blanks were 6.4 ± 1.1 pg and 2.0 ± 0.4 pg for Re and Os, respectively. Absolute uncertainties (2σ) are derived from error propagation of uncertainties in Re and Os mass spectrometer measurements, blank abundances and isotopic compositions, spike calibrations.

3.2. In situ laser ICP-MS trace element analyses

Pyrite grains used for the LA-ICP-MS spot analyses are observed by a reflected-light microscope to avoid possible contamination of mineral inclusions. Pyrite grains from the phyllic alteration are subhedral crystals (Fig. 3g). Pyrite from the potassic alteration is anhedral and is in most cases associated with chalcopyrite or native gold (Fig. 3h and i).

Table 1
Re-Os isotopic data for auriferous pyrite from the J1 orebody of the Jinchang Cu-Au deposit.

Sample no.	Weight (g)	Total Re (ppb)	2σ	^{187}Re (ppb)	2σ	^{187}Os (ppb)	2σ	Common Os (ppb)	2σ	^{187}Re/^{188}Os	2σ	^{187}Os/^{188}Os	2σ	$(^{187}Os/^{188}Os)_i$
JI-6-2	3.0175	1.48	0.19	0.93	0.12	0.002	0.001	0.014	0.001	512	76	0.99	0.08	0.02
JI-7-4	1.0064	7.65	0.63	4.79	0.39	0.009	0.001	0.038	0.006	956	176	1.83	0.31	0.01
JI-8-1	1.0351	7.10	0.54	4.44	0.34	0.009	0.002	0.022	0.005	1525	359	3.19	0.72	0.29
JI-8-5	0.5004	18.9	1.8	11.8	1.2	0.022	0.003	0.037	0.004	2443	366	4.52	0.53	−0.12
JI-8-7	1.0014	4.62	0.71	2.89	0.44	0.006	0.002	0.017	0.003	1345	313	2.65	0.48	0.09

Notes: Initial Os isotope ratios $(^{187}Os/^{188}Os)_i$ are calculated using an age of 114 Ma.

Trace element contents of pyrite were determined by an Agilent 7700× quadrupole ICP-MS coupled to a Photon Machines Excite Excimer laser ablation system at the Nanjing Focums Technology Co. Ltd. In order to enhance the sensitivity and lower the instrument background, two routine pumps were used for the vacuum system. Each analysis was performed by 40 μm diameter ablating spots at 8 Hz with energy of ~5 mJ per pulse for 40 s after measuring the gas blank for 15 s. Sample signal intensity data were converted to concentrations on basis by calibration against standard analyses of USGS GSE-1G, internal normalization to 100% total element abundance (Halicz and Günther, 2004). The precision of each analysis is better than 25% for most element (>1 ppm).

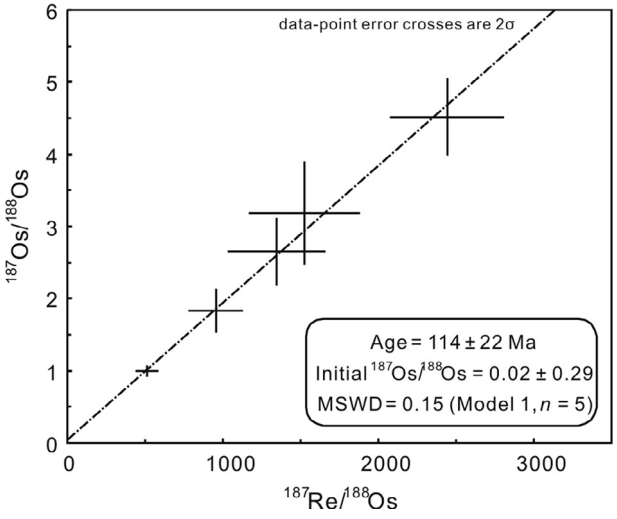

Fig. 4. Re-Os isochron plot of auriferous pyrite from the Jinchang Cu-Au deposit. The analytical data were processed by ISOPLOT software Version 3.27.

4. Analytical results

4.1. Re-Os isotopes of pyrite

Re-Os data of the five pyrite separates are listed in Table 1. Pyrite samples from the Jinchang Cu-Au deposit contain 1.48–18.9 ppb Re and 0.014–0.038 ppb common Os. ^{187}Re/^{188} Os ratios vary widely from 512 to 2443, with ^{187}Os/^{188}Os ratios ranging from 0.99 to 4.52. Regression of the Re-Os data (n = 5) yields an isochron age of 114 ± 22 Ma (2σ, MSWD = 0.15; Fig. 4). The calculated initial Os isotope ratios using an age of 114 Ma range from 0.01 to 0.29 (Table 1).

4.2. Trace elements of pyrite

In situ LA-ICP-MS spot analytical results of pyrite from the Jinchang deposit are given in the Appendix A. The average values and standard deviations of trace element contents in pyrite are listed in Table 2. In general, all of the pyrite grains contain <0.01–4.53 ppm Au with an average of 0.35 ppm and variable As from 0.53 to ~4519 ppm with an average of 497 ppm. Tellurium, Ag, Bi and Se contents are commonly less than 10 ppm. Copper, Pb, and Zn contents are up to ~1000, ~1500, and ~3500 ppm, respectively (Table 2). Cobalt and Ni contents are highly variable, ranging from

Table 2
LA-ICP-MS results for trace elements (in ppm) in pyrite from the Jinchang Cu-Au deposit.

Sample location	Sample no.		Co	Ni	Cu	Zn	As	Ag	Se	Sb	Te	Au	Pb	Bi	Co/Ni
	DL[a]		0.018	0.073	0.074	0.694	0.932	0.018	0.894	0.043	<0.001	<0.001	0.024	0.01	
80 m level	JI-0803(2)	ave (n = 6)[b]	0.05	126	324	750	1977	3.89	1.03	21.4	0.44	1.33	249	0.30	
		stdev	0.05	206	482	1518	1843	5.15	0.11	27.0	0.33	1.72	267	0.17	
	J1-6-2	ave (n = 3)	0.04	0.84	59.3	3.71	2949	10.3	b.d.l	125	0.66	3.49	1132	0.02	0.04
		stdev	0.01		13.0	1.48	713	4.0		12	0.25	1.00	414	0.00	
30 m level	JI-0804	ave (n = 10)	683	273	0.21	b.d.l	620	b.d.l	2.19	0.13	1.23	0.04	0.42	0.07	5.99
		stdev	1081	218	0.07		1224		0.64		2.95	0.06	0.37	0.09	12.6
	JI-0701(1)	ave (n = 9)	1730	102	0.17	b.d.l	90.3	0.02	1.82	0.11	0.27	0.02	1.10	0.29	37.1
		stdev	1773	111	0.07		152.5		0.92	0.05	0.42	0.02	1.57	0.31	72.3
−20 m level	J1-8-1	ave (n = 1)	369	156	b.d.l	0.72	1118	b.d.l	b.d.l	b.d.l	15.7	0.04	0.17	0.74	2.37
		stdev													
	JI-7-9	ave (n = 9)	840	23.6	0.37	b.d.l	32.5	b.d.l	2.01	b.d.l	0.40	0.03	0.03	0.39	106
		stdev	958	22.7	0.19		14.1		0.76		0.27	0.03		0.40	107
	J1-8-5	ave (n = 10)	1148	331	1.13	2.42	82.7	0.08	3.37	0.14	3.94	0.13	0.34	1.90	4.55
		stdev	1233	303	0.65		73.0	0.02	2.01	0.08	5.29	0.11	0.24	1.38	3.89
	J1-8-7	ave (n = 10)	1036	66.4	1.25	1.28	95.9	0.07	1.51	0.13	2.36	0.06	1.26	2.21	17.3
		stdev	1091	34.3	0.68	0.32	83.1	0.05	0.57	0.14	2.01	0.03	1.43	2.17	15.0

Abbreviation: D.L. = detection limit, ave = average, stdev = standard deviation, b.d.l = below detection limit.

[a] Detection limit (D.L.) = $3 \times \sigma^i_{background} \times C^i_{RM}/cps^i_{RM}$, where $\sigma^i_{background}$ is the standard deviation of multiple determinations of element i in the background, C^i_{RM} and cps^i_{RM} are concentration and peak intensity of element i in the reference material, respectively.

[b] Numbers in parenthesis represent the number of analyzed spots.

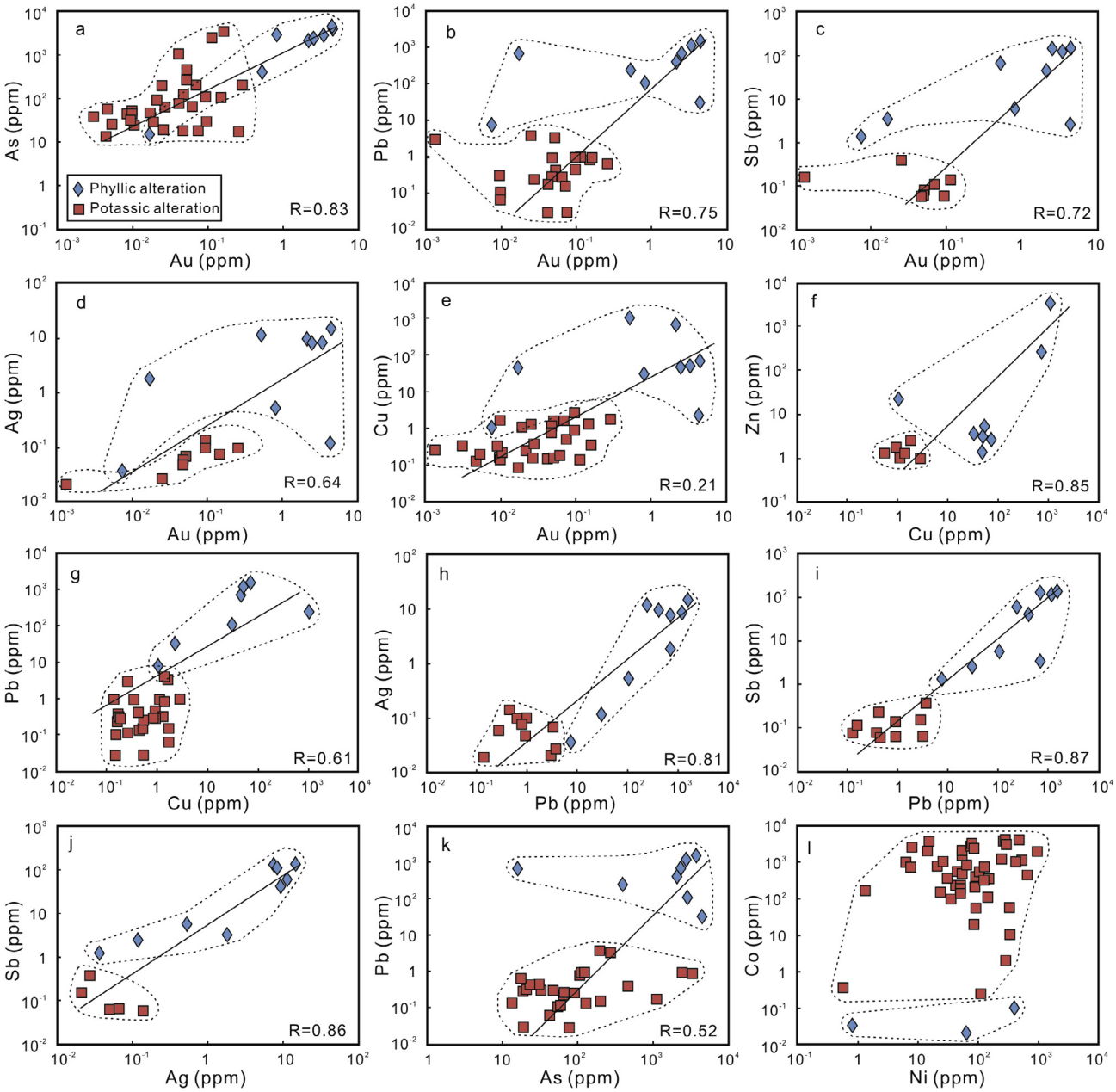

Fig. 5. Binary plot showing the correlation among elements Au, As, Pb, Sb, Zn, Cu, Ag, Co and Ni, also showing compositional differences of pyrite from phyllic and potassic alteration stages.

below the detection limits to several thousands of ppm. The Co/Ni ratios of pyrite range from <0.1 to 40 (Table 2).

There are positive correlations of Au with As, Pb, Sb, and Ag (correlation coefficient R = 0.64–0.83; Fig. 5a–d). Gold has a weak correlation with Cu (Fig. 5e). Copper is positively correlated with Zn and Pb, with correlation coefficients of 0.85 and 0.61, respectively (Fig. 5f and g). Well positive correlations are for elements Ag, Sb and Pb (R = 0.81–0.87) (Fig. 5h–j). Arsenic also shows a weak correlation with Pb (R = 0.52) (Fig. 5k). There is no obvious correlation between Co and Ni (Fig. 5l). Pyrite from the phyllic and potassic alteration stages has different trace element compositions. Pyrite from the phyllic alteration stage contains higher Au, As, Pb, Sb, Ag, Cu, Zn but lower Co, Ni, Se and Bi than that from potassic alteration stage (Figs. 5 and 6). In the As-Au plot, pyrite from these two stages defines different fields (Fig. 7). In the plot of Co vs. Ni, most of pyrite grains from the potassic alteration stage lie in the field of "volcanogenic" and "hydrothermal" fields (Fig. 8).

5. Discussion

5.1. Age of gold mineralization

Numerous geochronological data for the Jinchang Cu-Au deposit have been reported (Jia et al., 2008; Qing et al., 2012; Zhang et al., 2013), but all of them were obtained from indirect dating methods. For example, sericite from the Au-mineralized phyllic-altered granodiorite and granite porphyry has Rb-Sr ages of 110 ± 4 Ma and 107 ± 5 Ma, respectively (Zhang et al., 2013). Quartz from Au-bearing quartz-pyrite veins has Ar-Ar ages of 122.53 ± 0.88 Ma (Jia et al., 2008) and 119 ± 5 Ma (Qing et al., 2012). Sphalerite from Au-bearing quartz-sulfide veins has an Ar-Ar isochron age of 129 ± 0.8 Ma (Qing et al., 2012).

Sericite, quartz, and sphalerite are not Au-bearing minerals, and thus can only represent the alteration age rather than the mineralization age. As the main Au-bearing mineral, pyrite can provide the

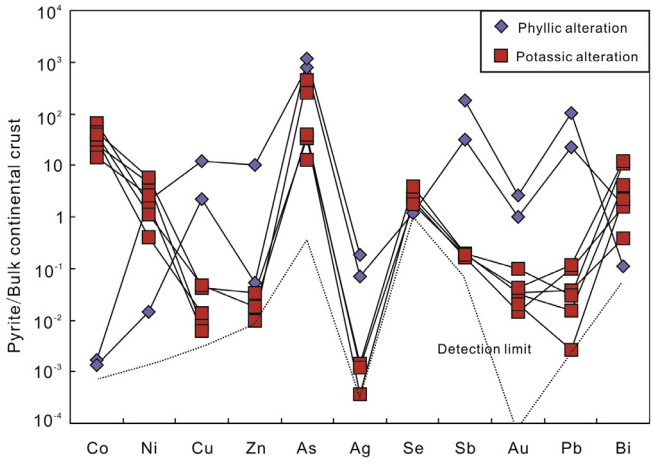

Fig. 6. Bulk continental crust normalized trace element diagram for pyrite from the phyllic and potassic alteration stages. Normalization values are form Rudnick and Gao (2003).

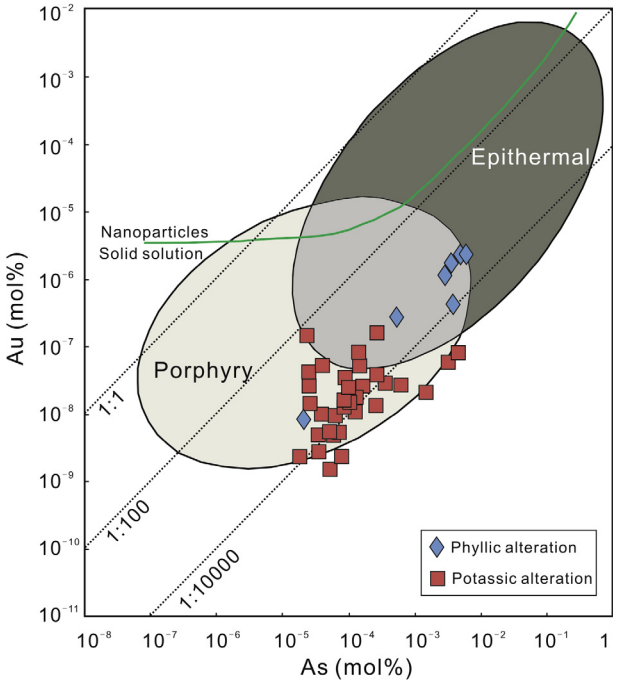

Fig. 7. Au-As distribution diagram for pyrite from the Jinchang deposit (log-log scale; in mol.%). The boundaries of different deposits are referenced to Deditius et al. (2014). The green line is defined as the solid solubility limit by Reich et al. (2005). (For interpretation of the references to color in this figure legend, the reader is referred to the web version of this article.)

direct mineralization age. Auriferous pyrite has a Re-Os age of 114 ± 22 Ma, which reveals the direct timing of gold mineralization. This age is in agreement with previous Ar-Ar and Rb-Sr ages of 107–129 Ma within uncertainties. Therefore, we suggest that the Au mineralization of the Jinchang Cu-Au deposit may have occurred at ~114 Ma.

5.2. Nature and evolution of hydrothermal fluids

The nature of the ore-forming fluids in porphyry system can be recorded by chemical composition of sulfides and fluid inclusions in quartz veins. Pyrite from the potassic and phyllic alteration stages has different trace element contents. Pyrite from the phyllic alteration stage has higher trace element (except for Co and Ni)

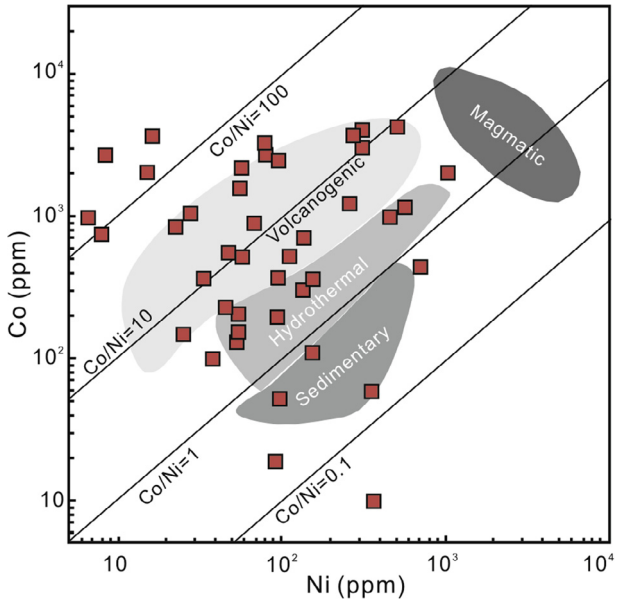

Fig. 8. Co-Ni distribution diagram for pyrite from the potassic alteration stage of the Jinchang deposit. Pyrite from the phyllic alteration stage has very low Co content plotting outside the diagram. The boundaries of different origins are referenced to Bralia et al. (1979) and Bajwah et al. (1987). "Volcanogenic" means volcanic-hosted deposits, and these deposits are genetically related to the host volcanic rocks. "Magmatic" means magmatic Ni-Cu deposits such as Sudbury where sulfides crystallized directly from the magma.

contents than that from the potassic alteration stage (Figs. 5 and 6). This trend is similar to pyrite from the Altar porphyry-epithermal Cu-Au deposit (Maydagán et al., 2013). Butler and Rickard (2000) demonstrated that pyrite formed rapidly at a low temperature (<150 °C) was more likely fine-grained than that formed more slowly at a higher temperature (>200 °C) from hydrothermal fluids. The high-temperature hydrothermal pyrite is expected to be less enriched in trace elements due to the higher temperature, whereas a lower temperature allows the trace elements to be partitioned into separate sulfide phases rather than incorporated into pyrite lattice (Butler and Rickard, 2000; Large et al., 2009). The compositional differences of pyrite from these two alteration stages may reflect the various fluid nature and fluid compositions, consistent with the results from the fluid inclusion data.

Fluid inclusions in the Jinchang deposit display homogenization temperatures ranging from ~171 to 590 °C and salinity of 1–70 wt. % NaCl equivalent (Wang et al., 2007, 2011; Men et al., 2008; Zhang et al., 2014, unpublished data). The high temperature and high salinity fluid characteristics of the Jinchang deposit are similar to the other Cu-(Au) porphyry systems related to high-temperature unmixing saline magmatic fluids (e.g., Ulrich et al., 2001; Harris and Golding, 2002; Redmond et al., 2004; Heinrich, 2005, 2007; Bouzari and Clark, 2006; Cooke et al., 2011; Maydagán et al., 2015). Fluid inclusions of the potassic stage have homogenization temperatures of ~200–590 °C (average ~329 °C) and salinities of ~5–70 wt.% (average ~18.6 wt.%) NaCl equivalent, slightly higher than the homogenization temperatures of ~171–550 °C (average ~303 °C) and salinities of ~1–36 wt.% (average ~14.2 wt.%) NaCl equivalent for the phyllic stage (Wang et al., 2007, 2011; Men et al., 2008; Zhang et al., 2014, unpublished data). Different fluid nature between the potassic and phyllic alteration stages may be due to the dilution of the magmatic fluids with meteoric water (Henley and McNabb, 1978) and the thermal collapse of the magmatic-hydrothermal system (Shinohara and Hedenquist, 1997). When the magma fluid mixing with meteoric water cooled, HCl dissociated and SO_2 proportioned into H_2SO_4 and H_2S (Seedorff

et al., 2005). Acid fluids resulted in phyllic alteration superimposed on the potassic alteration and carried significant concentrations of metals (Seedorff et al., 2005). The increasing H_2S caused voluminous sulfide precipitation and quartz-pyrite-chalcopyrite veins in the potassic stage followed by Au-bearing quartz-sulfide veins in the phyllic stage.

Pyrite is the main host of Au in the Jinchang deposit. Small amounts of Au could be incorporated into the pyrite lattice when other elements, such as As, Te and Sb, distorted the pyrite lattice to allow Au to enter (Cook et al., 2009). Previous studies have shown that the high concentrations of Au that can be incorporated into pyrite always relate to the function of As concentration (Reich et al., 2013; Deditius et al., 2014). Pyrite formed in different environments of ore formation has different Au-As compositional fields (Deditius et al., 2014). Good correlation between Au and As in pyrite (Fig. 5a) and the Au-As plot (Fig. 7) indicates Au occurs as solid solution in pyrite. Pyrite from the potassic alteration stage has Au and As contents similar to porphyry systems, whereas that from phyllic alteration stage has element contents similar to the transitional field between porphyry and epithermal systems (Fig. 7). We suggest that the ore-forming fluids for pyrite formation may have been evolved continuously for these two stages. Moreover, the positive correlations among elements Au, As, Pb, Sb and Ag in pyrite from these two stages (Fig. 5) also indicate a continuous evolution process. Porphyry Cu deposits are associated with high-sulfidation systems located laterally or superimposed upon the porphyry deposits (Sillitoe, 2010; Heinrich, 2005; Waters et al., 2011). Both porphyry and epithermal mineralization types are the results of gradual retraction of isotherms around cooling hydrous plutons in similar tectonic and hydrologic environments (Heinrich, 2005). Magmatic fluids are produced at increasing depths with increasing vapour contraction, leading to the typical overprinting of potassic, phyllic and advanced argillic alteration and their related ore types (Heinrich, 2005). Considering the different nature of ore-forming fluids between potassic and phyllic alteration stages indicated by fluid inclusions, we suggest that the compositional differences of pyrite from these two stages are the results of both physical and chemical changes of magmatic fluids.

5.3. Origin of the Jinchang deposit

Previous studies of stable isotopes and fluid inclusions are available for the Jinchang deposit. Quartz from ores of the Jinchang Cu-Au deposit has $\delta^{18}O_{SMOW}$ and δD_{SMOW} values varying from −0.7‰ to +10.1‰ and from −99‰ to −70‰, respectively (Zhang et al., 2013 and references therein), indicating that the ore-forming fluids were mainly exsolved from magmas with minor amounts of meteoric water. Sulfur isotope composition of pyrite ($\delta^{34}S_{CDT}$ values) ranges from 1.1‰ to 8.8‰ (Mu et al., 2000; Li et al., 2003; Jia et al., 2008), indicating that the sulfur was possibly magmatic/volcanic in origin. Pyrite and galena from quartz-sulfide veins of the deposit have $^{206}Pb/^{204}Pb$ ratios of 17.3–18.5, $^{207}Pb/^{204}Pb$ ratios of 15.2–15.6 and $^{208}Pb/^{204}Pb$ ratios of 37.4–38.4 (Mu et al., 2000), characteristic of a lower crust. Fluid inclusion data suggest that the Jinchang deposit was closely related to an oxidized intrusion (Zhang et al., 2014).

Rhenium contents of pyrite can reflect the source of the ore-forming fluids to some extent. Pyrite acts as an efficient Re sink as it can preferentially take up large quantities of Re from ore-forming fluids (Frei et al., 1998; Huang et al., 2013a). Pyrite from different types of porphyry deposits has different Re contents (Figs. 9 and 10), indicating the complex behavior of Re in the porphyry system (e.g., Mathur et al., 2000a,b, 2005; Barra et al., 2003; Cardon et al., 2008; Liu et al., 2012; Ying et al., 2014; Zimmerman et al., 2014). Because pyrite was commonly associated with molybdenite in many porphyry deposits, Re of pyrite can be affected by the associated molybdenite, less for Os contents of pyrite (Selby et al., 2009). Pyrite from Cu-Mo porphyry deposits has a wider range of Re contents than those from Cu-Au and Cu porphyry deposits (Fig. 9), which may be related to the proportion of molybdenite in mineral assemblage of Cu-Mo deposits. Because molybdenite can host ppm level Re, minor molybdenite precipitation can significantly affect Re in associated pyrite. In the Jinchang deposit, molybdenite is not present, precluding the effect of intergrown molybdenite on the Re content of pyrite. Previous studies have demonstrated that Fe- and Cu-rich fluids can enrich fluids Re more than W ± Pb ± Zn ± Au bearing fluids (Yang et al., 2011;

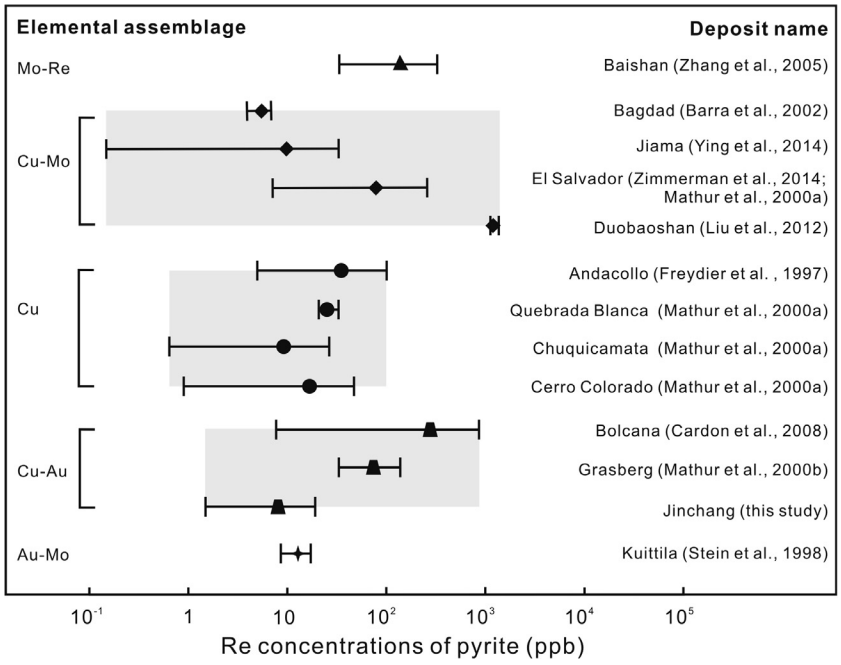

Fig. 9. Correlation diagram between Re concentration of pyrite and elemental assemblages of different porphyry deposits. The black filled symbols represent the average values of Re contents, whereas the error bars represent the minimum and maximum values. (See above-mentioned references for further information.)

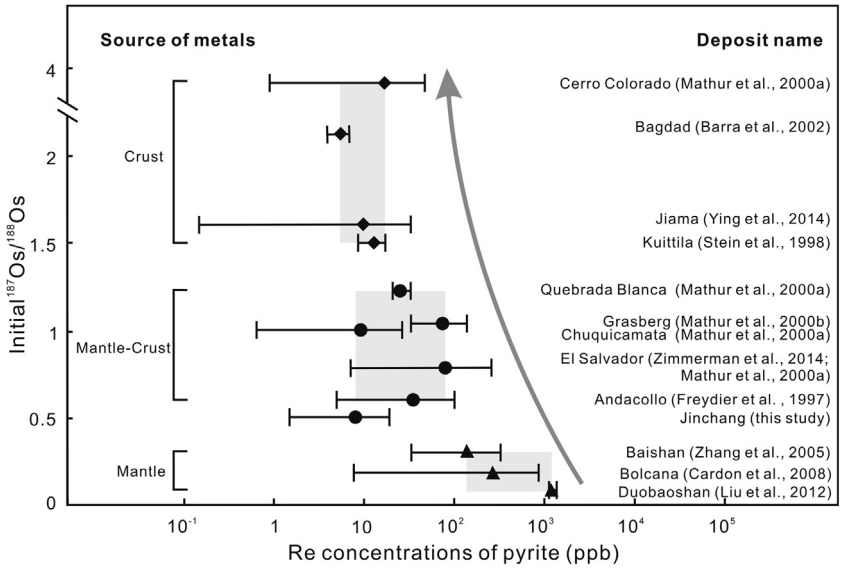

Fig. 10. Correlation diagram between Re concentration of pyrite and material sources of different porphyry deposits. Initial $^{187}Os/^{188}Os$ ratios for each deposit are calculated from the isochrones. Pyrite from Duobaoshan, Bolcano, Jinchang, Kuittila deposits doesn't have initial Os isotope ratios or has these values with large uncertainties, these deposits are thus plotted only according to Re contents. Their metal sources are inferred from other isotopes. The black filled symbols represent the average values of Re contents, whereas the error bars represent the minimum and maximum values. (See above-mentioned references for further information.)

Huang et al., 2013a). For the porphyry system, fluids are rich in Fe and Cu, precluding the effects of the nature of fluids on Re contents. Mao et al. (1999) showed that Re content of molybdenite would decrease from mantle-related deposits (hundreds of ppm) to I-type (several ppm) and S-type (ppm) granite-related deposits. Re contents and initial Os isotope ratios of pyrite from porphyry deposits define a rough trend that Re contents of pyrite decrease from a mantle-dominant source to crust-dominant source (Fig. 10). Re contents of pyrite from the Jinchang deposit are lower than those of mantle-sourced pyrite, but are similar to those of pyrite from the mixing source of mantle-crust and the crustal source (Fig. 10), implying that the Jinchang deposit may have had a mixing mantle-crust source or a crustal source.

Osmium and Cu should have similar chalcophile behavior in porphyry systems, and thus we can infer the source of Cu from understanding the source of Os (Mathur et al., 2000a,b; Barra et al., 2003; Cardon et al., 2008). The initial $^{187}Os/^{188}Os$ ratio from the pyrite isochron is 0.02 ± 0.29 (Fig. 4). The large uncertainty of the initial ratio makes it difficult to discuss the source of metals. But the calculated initial Os isotope ratios of individual samples can give some information about the origin of metals. Three pyrite samples have initial $^{187}Os/^{188}Os$ ratios of 0.01, 0.02, and 0.09 (Table 1), closer to typical mantle (~0.12–0.13) than crustal (~1.0–1.5) $^{187}Os/^{188}Os$ ratios (Walker and Morgan, 1989), indicating a dominantly mantle origin for the metals. One pyrite sample has an $^{187}Os/^{188}Os$ ratio of 0.29 (Table 1), indicating a significant crustal component for the source of Os in pyrite. However, because the radiogenic Os content of these pyrite samples is only about two or three times higher than the typical blank, this conclusion should be with caution.

Pyrite samples from the Jinchang deposit have lower common Os and higher Re/Os ratios than magmatic sulfides, similar to those of Lewisian lower crust (Fig. 11). The crustal source of pyrite is consistent with Pb isotope composition of sulfides (Zhang et al., 2013). Co/Ni ratios of pyrite can be used for examining the origin of sulfide deposits (Loftus-Hills and Solomon, 1967; Bralia et al., 1979; Bajwah et al., 1987). Pyrite samples from the Jinchang deposits have Co/Ni ratios similar to those from the volcanogenic and hydrothermal deposits, indicating a magmatic-hydrothermal origin (Fig. 8). The Re-Os isotope age of pyrite provides the direct

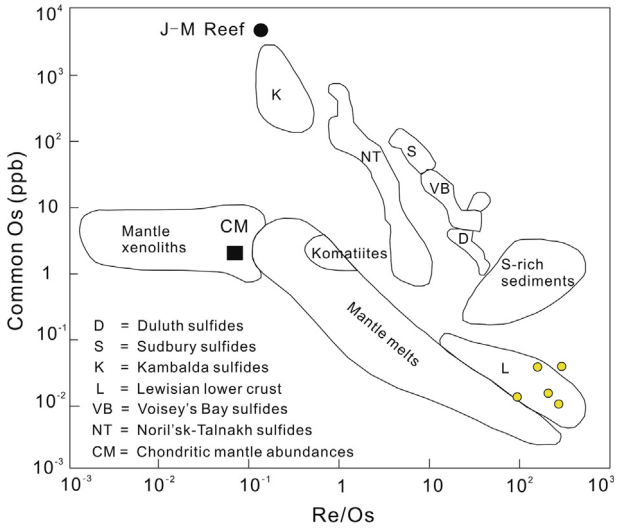

Fig. 11. Re/Os vs. common Os plot for auriferous pyrite from the Jinchang deposit (modified after Lambert et al., 2000).

evidence for correlating mineralization and granitic/dioritic porphyry due to their similar ages. Au and As contents of pyrite from this deposit are similar to those of porphyry-epithermal systems (Fig. 7). The ore-related granite porphyry was considered to be produced by partial melting of juvenile Proterozoic crust with notable input of mantle components (Zhang et al., 2013). This is consistent with a mantle-crust mixing characteristic of initial Os isotope composition. Thus, we suggest that the Cretaceous granite porphyry was the main source of ore-forming materials.

5.4. Implication for regional mineralization

There are at least two episodes of magmatism in the study area, i.e. Early Jurassic (ca. 210–195 Ma) and Cretaceous (ca. 120–110 Ma) (Table 3 and Fig. 12). Our Re-Os age of pyrite and previous ages of alteration and mineralization indicate that Au mineralization at Jinchang occurred between 107 and 129 Ma (Fig. 12). These

Table 3
Summary of geochronological data from the Jinchang Cu-Au deposit.

Rock/Ore	Method	Mineral	Age (Ma)	Reference
Granodiorite	U–Pb	Zircon	195.1 ± 8.4	Zhang (2007)
Diorite	U–Pb	Zircon	209.5 ± 1.4	Zhao (2013)
Biotite monzogranite	U–Pb	Zircon	203 ± 4	Zhang et al. (2013)
Granophyric granite	U–Pb	Zircon	203 ± 3.6	Men et al. (2008)
Granophyric granite	U–Pb	Zircon	201 ± 3	Zhang et al. (2013)
Granophyric granite	U–Pb	Zircon	201 ± 3	Lu et al. (2009)
Granite porphyry	U–Pb	Zircon	113.5 ± 3.8	Qian et al. (2012)
Granite porphyry	U–Pb	Zircon	112.62 ± 0.85	Zhao (2013)
Granite porphyry	U–Pb	Zircon	110 ± 3	Zhang et al. (2013)
Diorite porphyry	U–Pb	Zircon	111.5 ± 1.2	Lu et al. (2009)
Diorite porphyry	U–Pb	Zircon	118.1 ± 1.6	Zhao et al. (2012)
Diorite porphyry	U–Pb	Zircon	116 ± 2	Zhao et al. (2012)
Altered granodiorite	Rb–Sr	Sericite	110 ± 4	Zhang et al. (2013)
Altered granite porphyry	Rb–Sr	Sericite	107 ± 5	Zhang et al. (2013)
Quartz-sulfide vein	Ar–Ar	Quartz	122.53 ± 0.88	Jia et al. (2008)
Quartz-sulfide vein	Ar–Ar	Quartz	119 ± 5	Qing et al. (2012)
Quartz-sulfide vein	Ar–Ar	Sphalerite	129 ± 0.8	Qing et al. (2012)
Quartz-sulfide vein	Re–Os	Pyrite	114 ± 22	This study

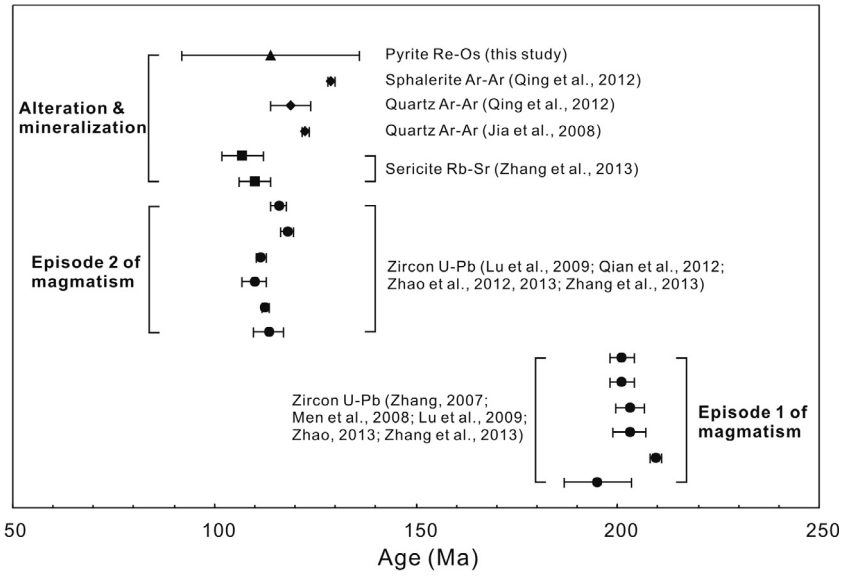

Fig. 12. Temporal correlation diagram for magmatism and mineralization in the Jinchang Cu-Au deposit.

ages demonstrate that the mineralization was not related to the early Jurassic magmatism, but the Cretaceous granitic magmatism (Fig. 12).

In NE China, there are mainly two episodes of porphyry related mineralization events, which are related to different tectonic and magmatic events (Fig. 1a). Since the Jurassic (ca. 170–135 Ma), this region was in an intraplate orogeny stage with extensive magmatism and back-arc extension caused by the low-angle subduction of the Paleo-Pacific plate (Zeng et al., 2015). Numerous porphyry Cu-Mo-Au, Cu and Mo-Cu deposits are proposed to be associated with partial melting of subducted Paleo-Pacific plate and formed along the suture zones or the major tectonic boundaries where plate breakup and plate windows may have occurred (Li et al., 2008; Mao et al., 2014 and references therein). Porphyry Mo deposits in a back-arc extension belt are genetically related to I-type granitic rocks (Mao et al., 2011a,b; Nie et al., 2011; Zeng et al., 2013). Cretaceous large-scale lithospheric thinning, delamination and mantle upwelling were triggered by the changing direction of the Paleo-Pacific plate from oblique to parallel to the continent margin (e.g., Wang et al., 2006; Maruyama et al., 2007; Pirajno et al., 2009; Wu et al., 2011; Zhang et al., 2013; Goldfarb et al., 2014; Mao et al., 2014). The extensive Cretaceous magmatic rocks in eastern China (Wu et al., 2005), extensional basins along the eastern Asian continental margin (Ren et al., 2002) and associated Au metallogeny (Goldfarb et al., 2014; Mao et al., 2014) indicate an extensional tectonic regime during large scale mantle upwelling at the Early Cretaceous. Porphyry Cu-Au deposits and related granitic rocks were possibly associated with residual subducted slab fragments (Mao et al., 2014), whereas porphyry Mo deposits in the Dongqinling-Dabie orogenic belt are genetically related to S-type granites and are probably derived from an upper crustal source (Mao et al., 2011a,b; Zeng et al., 2013).

Based on the regional geological background, we suggest that the Jinchang deposit probably formed in an extensional tectonic setting associated with the extensive Cretaceous granitic magmatism. These granitic rocks were produced by partial melting of the juvenile Proterozoic lower crust with minor mantle components and wall rock contaminants. Mantle upwelling might have provided not only heat for the melting but also fluids that scavenge metals from the lower crust and transfer them to the shallow upper crust (Zhang et al., 2014). The continuous process of mantle upwelling, reactivation of deep-seated faults,

mantle-crust interaction and crust melting was most likely induced by the changing subduciton angle of the Paleo-Pacific plate.

6. Conclusions

Re-Os isotope analyses of the auriferous pyrite from the Jinchang Cu-Au deposit give an age of 114 ± 22 Ma, representing the direct mineralization age. The Cu-Au mineralization was related to the Cretaceous granitic magmatism. Different trace element compositions of pyrite between potassic and phyllic alteration stages may be due to the changing physical and chemical conditions during the ore-forming process. Gold and As contents and Co/Ni values of pyrite indicate a magmatic-hydrothermal origin. Pyrite Re and Os contents and their isotope compositions suggest a crustal source or mixed mantle-crust source. According to the tectonic evolution of NE China, we suggest that the Jinchang porphyry Cu-Au deposit was closely related to the Early Cretaceous subduction of the Paleo-Pacific plate.

Acknowledgements

This study was funded by the program of gold geology research from Gold Geological Institute of China People's Armed Force Police Force (20140404005). We thank the staff of No. 1 Party of Gold Geology, China People's Armed Force Police Force for the field work in the Jinchang Mine. Two anonymous reviewers, Prof. Borming Jahn and Mei-Fu Zhou are thanked for their constructive comments and suggestions which have significantly improved the manuscript.

Appendix A

Full analytical results (in ppm) for Laser Ablation ICP–MS of pyrite from the Jinchang Cu-Au deposit.

Lab No.	Spot No.	Co	Ni	Cu	Zn	As	Ag	Se	Sb	Te	Au	Pb	Bi
Detection limit		0.018	0.073	0.074	0.694	0.932	0.018	0.894	0.043	<0.001	<0.001	0.024	0.01
Py0429F28	JI-0803(2)-02	0.1	431	33	3.55	2853	0.53		5.63	0.2	0.82	106	0.55
Py0429F29	JI-0803(2)-03		2.47	755	265	2030	9.39	0.95	40.3	0.24	2.15	406	0.32
Py0429F30	JI-0803(2)-04	0.02		2.39		4519	0.12		2.47	1.02	4.45	30.7	0.14
Py0429F31	JI-0803(2)-05	0.02	68.2	48.6	1.39	15.7	1.8		3.29	0.39	0.02	703	0.43
Py0429F32	JI-0803(2)-06		0.91	1.07	22.2		0.04	1.11	1.26	0.36	0.01	7.49	0.19
Py0429F36	JI-0803(2)-10			1104	3458	400	11.5		59.6		0.53	243	0.18
Py0422A39	J1-6-2-08	0.03	0.84	74.1	2.63	3733	14.9		133	0.37	4.53	1525	0.02
Py0422A40	J1-6-2-09			49.7	3.09	2339	7.63		130	0.77	2.54	699	
Py0422A41	J1-6-2-10	0.04		54.2	5.4	2773	8.35		112	0.84	3.42	1172	0.02
Py0429F39	JI-0804-01	997	458	0.19		32.4		2.26		0.25	0.01	0.29	0.13
Py0429F40	JI-0804-02	447	702	0.16		54.4		2.15		0.06	0.01	0.1	
Py0429F41	JI-0804-03	3024	311	0.28		60.2		1.07				0.11	
Py0429F42	JI-0804-04	0.04		0.36		3376				0.21	0.16	0.88	
Py0429F43	JI-0804-05	2196	56.8	0.16		64.5					0.03	0.23	
Py0429F44	JI-0804-06	10.4	365	0.13		39.5		2.99		0.09	0.01		
Py0429F45	JI-0804-07	133	53.1	0.25		93.7				7.92	0.02		
Py0429F46	JI-0804-08	2.03	305	0.21		26.2		2.15		0.07	0.01		
Py0429F47	JI-0804-09	19.7	91.6	0.14		2428			0.13		0.11	0.91	
Py0429F48	JI-0804-10	0.25	118			20.7		2.53					
Py0429F03	JI-0701(1)-01	1059	27.7	0.09		42				0.05			0.03
Py0429F04	JI-0701(1)-02	3690	273	0.15		78.2		3.12		0.43	0.04	0.03	0.55
Py0429F05	JI-0701(1)-03	4100	302	0.13		58.7		2.43		0.02	0.01		0.02
Py0429F06	JI-0701(1)-04	2657	80.6	0.08		31.1		1.05					
Py0429F07	JI-0701(1)-05	201	93.8			9.59		1.4					
Py0429F08	JI-0701(1)-06	151	25			14				0.02	0		
Py0429F09	JI-0701(1)-07	3662	16.2	0.25		25.7		1.08			0.01		
Py0429F10	JI-0701(1)-08	53.8	97.1	0.17		463			0.08	0.03	0.05	0.38	
Py0429F11	JI-0701(1)-09	0.36	0.59	0.26			0.02		0.15	1.06		2.9	0.57
Py0422A53	J1-8-1-08	369	156		0.72	1118				15.7	0.04	0.17	0.74
Py0429F15	JI-7-9-01	2122	15.2	0.09		47.7				0.39	0.02		
Py0429F16	JI-7-9-02	177	1.4			42.5		3.31		0.76			
Py0429F17	JI-7-9-03	0.46		0.51		46.1		1.83					
Py0429F18	JI-7-9-04	102	37.9	0.56		18.4		1.9					
Py0429F20	JI-7-9-06	760	7.98	0.37		45.7					0.01		
Py0429F21	JI-7-9-07	526	57.7	0.1		14.8				0.04			
Py0429F22	JI-7-9-08	2697	8.37	0.36		39.2		1.73		0.3	0		
Py0429F23	JI-7-9-09	185	54	0.55		18.8		1.29		0.65	0.08	0.03	0.68
Py0429F24	JI-7-9-10	990	6.6	0.38		19.7				0.26	0.03		0.11
Py0422A04	J1-8-5-02	4240	510	1.76		202		1.4	0.11		0.07	0.16	
Py0422A05	J1-8-5-03	2035	1037	1.87	2.43	201		2.66		17.5	0.29		

(*continued on next page*)

Appendix A (*continued*)

Lab No.	Spot No.	Co	Ni	Cu	Zn	As	Ag	Se	Sb	Te	Au	Pb	Bi
Py0422A06	J1-8-5-04	113	155			17.7	0.1	6.11		1.47	0.26	0.62	4.36
Py0422A07	J1-8-5-05	532	112	0.43		22.4		1.26	0.23	2.22		0.42	3.28
Py0422A08	J1-8-5-06	483	111	0.2		67		5.05		1.84	0.06	0.27	1.45
Py0422A09	J1-8-5-07	61	355	0.45		126		4.99	0.08	2.61		0.13	0.87
Py0422A10	J1-8-5-08	1171	567	1.49		107	0.08	1.03		5.79	0.15	0.8	1.45
Py0422A11	J1-8-5-09	1235	261	1.74		43.5		4.43		2.13	0.01	0.06	
Py0422A13	J1-8-5-11	715	137	1.41		21.8				1.98		0.3	1.33
Py0422A14	J1-8-5-12	900	68.1	0.88		19.1	0.06				0.05	0.28	0.58
Py0422A18	J1-8-7-01	373	33.5	1.17	1.27	124	0.05		0.06	3.51	0.05	0.93	2.73
Py0422A19	J1-8-7-02	2563	95.9	0.98		30.4	0.14		0.06	2.3	0.1	0.45	4.77
Py0422A20	J1-8-7-03	3292	79.1	0.94	1.85	46.5		2.07				0.29	1.11
Py0422A22	J1-8-7-05	563	47.3	1.43	1.27	195	0.03		0.38		0.03	3.74	1.94
Py0422A23	J1-8-7-06	1587	55.6	1.13	1.01	29.4				0.3	0.02		0.55
Py0422A24	J1-8-7-07	233	45.6	1.17		46.6		0.92	0.06	1.58			0.15
Py0422A25	J1-8-7-08	210	54.8	1.68		272	0.07		0.06	6.07	0.05	3.3	6.61
Py0422A26	J1-8-7-09	308	135	2.92	0.97	110	0.1	1.53		0.28	0.09	0.95	1.41
Py0422A27	J1-8-7-11	856	22.5	0.53	1.32	13.5	0.02					0.14	
Py0422A28	J1-8-7-12	377	95.3	0.57		91.7				2.47		0.25	0.63

Notes: Blank in the data table denotes the content of the element is below detection limit.

References

Arne, D.C., Bierlin, F.P., Morgan, J.W., Stein, H.J., 2001. Re-Os dating of sulfides associated with gold mineralization in central Victoria, Australia. Econ. Geol. 96, 1455–1459.

Bajwah, Z.U., Seccombe, P.K., Offler, R., 1987. Trace element distribution Co: Ni ratios and genesis of the Big Cadia iron-copper deposit, New South Wales, Australia. Miner. Deposita 22, 292–300.

Barra, F., Ruiz, J., Mathur, R., Titley, S., 2003. A Re–Os study of sulfide minerals from the Bagdad porphyry Cu–Mo deposit, northern Arizona, USA. Miner. Deposita 38, 585–596.

Bouzari, F., Clark, A.H., 2006. Prograde evolution and geothermal affinities of a major porphyry copper deposit: the cerro colorado hypogene protore, I Region, Northern Chile. Econ. Geol. 101, 95–134.

Bralia, A., Sabatini, G., Troja, F., 1979. A revaluation of the Co/Ni ratio in pyrite as geochemical tool in ore genesis problems: evidences from southern Tuscany pyritic deposits. Miner. Deposita 14, 353–374.

Butler, I.B., Rickard, D., 2000. Framboidal pyrite formation via the oxidation of iron (II) monosulfide by hydrogen sulphide. Geochim. Cosmochim. Acta 64, 2665–2672.

Cardon, O., Reisberg, L., Andre-Mayer, A.S., Leroy, J., Milu, V., Zimmermann, C., 2008. Re-Os systematics of pyrite from the Bolcana porphyry copper deposit, Apuseni Mountains, Romania. Econ. Geol. 103, 1695–1702.

Cook, N.J., Ciobanu, C.L., Mao, J., 2009. Textural control on gold distribution in As-free pyrite from the Dongping, Huangtuliang and Hougou gold deposits, North China Craton (Hebei Province, China). Chem. Geol. 264, 101–121.

Cooke, D.R., Deyell, C.L., Waters, P.J., Gonzales, R.I., Zaw, K., 2011. Evidence for magmatic-hydrothermal fluids and ore-forming processes in epithermal and porphyry deposits of the Baguio District, Philippines. Econ. Geol. 106, 1399–1424.

Chen, J.R., Li, H.G., Jin, B.Y., Wu, Y.H., Wang, Y.Z., Yu, W.Q., 2002. Geological features and the deep metallogenic forecast of the No. J-1 gold body in the Jinchang gold deposit, Heilongjiang. Gold Geol. 8, 8–12 (in Chinese with English abstract).

Chen, Y.J., Guo, G.J., Li, X., 1998. Metallogenic geodynamic background of Mesozoic gold deposits in granite-greenstone terrains of North China Craton. Sci. China 41, 113–120.

Chen, Y.J., Xiao, W.J., Zhang, J.J., 2008. Ore-system as a geodynamic probe. Geol. China 35, 1059–1073 (in Chinese with English abstract).

Chen, Y.J., Zhai, G.M., Jiang, S.Y., 2009. Significant achievements and open issues in study of orogenesis and metallogenesis surrounding the North China continent. Acta Petrol. Sinica 25, 2695–2726 (in Chinese with English abstract).

Cioacă, M.E., Munteanu, M., Qi, L., Costin, G., 2014. Trace element concentrations in porphyry copper deposits from Metaliferi Mountains, Romania: a reconnaissance study. Ore Geol. Rev. 63, 22–39.

Deditius, A.P., Reich, M., Kesler, S.E., Utsunomiya, S., Chryssoulis, S.L., Walshe, J., Ewing, R.C., 2014. The coupled geochemistry of Au and As in pyrite from hydrothermal ore deposits. Geochim. Cosmochim. Acta 140, 644–670.

Frei, R., Nägler, T.F., Schönberg, R., Kramers, J.D., 1998. Re-Os, Sm-Nd, U-Pb, and stepwise lead leaching isotope systematics in shear-zone hosted gold mineralization: genetic tracing and age constraints of crustal hydrothermal activity. Geochim. Cosmochim. Acta 62, 1925–1936.

Freydier, C., Ruiz, J., Chesley, J., Mccandless, T., Munizaga, F., 1997. Re-Os isotope systematics of sulfides from felsic igneous rocks: Application to base metal porphyry mineralization in Chile. Geology 25, 775–778.

Goldfarb, R.J., Taylor, R.D., Collins, G.S., Goryachev, N.A., Orlandini, O.F., 2014. Phanerozoic continental growth and gold metallogeny of Asia. Gondwana Res. 25, 48–102.

Halicz, L., Günther, D., 2004. Quantitative analysis of silicates using LA-ICP-MS with liquid calibration. J. Anal. At. Spectrom. 19, 1539–1545.

Harris, A.C., Golding, S.D., 2002. New evidence of magmatic-fluid related phyllic alteration: implications for the genesis of porphyry Cu deposits. Geology 30, 335–338.

Henley, R.W., Mcnabb, A., 1978. Magmatic vapor plume and ground-water interaction in porphyry copper emplacement. Econ. Geol. 73, 1–20.

Heinrich, C.A., 2005. The physical and chemical evolution of low-salinity magmatic fluids at the porphyry to epithermal transition: a thermodynamic study. Miner. Deposita 39, 864–889.

Heinrich, C.A., 2007. Fluid-fluid interactions in magmatic-hydrothermal ore formation. Rev. Mineral. Geochem. 65, 363–387.

Huang, X.-W., Gao, J.-F., Qi, L., Zhou, M.-F., 2015. In-situ LA-ICP-MS trace elemental analyses of magnetite and Re–Os dating of pyrite: the Tianhu hydrothermally remobilized sedimentary Fe deposit, NW China. Ore Geol. Rev. 65, 900–916.

Huang, X.-W., Qi, L., Gao, J.-F., Zhou, M.-F., 2013a. First reliable Re-Os ages of pyrite and stable isotope compositions of Fe(-Cu) deposits in the Hami region, Eastern Tianshan Orogenic Belt, NW China. Resour. Geol. 63, 166–187.

Huang, X.-W., Zhao, X.-F., Qi, L., Zhou, M.-F., 2013b. Re-Os and S isotopic constraints on the origins of two mineralization events at the Tangdan sedimentary rock-hosted stratiform Cu deposit, SW China. Chem. Geol. 347, 9–19.

Huang, X.-W., Zhou, M.-F., Qi, L., Gao, J.-F., Wang, Y.-W., 2013c. Re-Os isotopic ages of pyrite and chemical composition of magnetite from the Cihai magmatic-hydrothermal Fe deposit, NW China. Miner. Deposita 48, 925–946.

Jia, D.C., Hu, R.Z., Yan, L., Qiu, X.L., 2004. Collision belt between the Khanka block and the North China block in the Yanbian region, Northeast China. J. Asian Earth Sci. 23, 211–219.

Jia, G.Z., Chen, J.R., Yang, Z.G., Bian, H.Y., Wang, Y.Z., Liang, H.J., Jin, T.H., Li, Z.H., 2008. Geology and genesis of the superlarge Jinchang gold deposit, NE China. Acta Geol. Sinica 82, 750–761.

Kerr, A., Selby, D., 2012. The timing of epigenetic gold mineralization on the Baie Verte Peninsula, Newfoundland, Canada: new evidence from Re-Os pyrite geochronology. Miner. Deposita 47, 325–337.

Kirk, J., Ruiz, J., Chesley, J., Titley, S., Walshe, J., 2001. A detrital model for the origin of gold and sulfides in the Witwatersrand basin based on Re-Os isotopes. Geochim. Cosmochim. Acta 65, 2149–2159.

Koglin, N., Frimmel, H.E., Lawrie Minter, W.E., Brätz, H., 2010. Trace-element characteristics of different pyrite types in Mesoarchaean to Palaeoproterozoic placer deposits. Miner. Deposita 45, 259–280.

Lambert, D.D., Foster, J.G., Frick, L.R., Li, C., Naldrett, A.J., 2000. Re-Os isotope systematics of the Voisey's Bay Ni-Cu-Co magmatic sulfide system, Labrador, Canada. Econ. Geol. 95, 867–888.

Large, R.R., Danyushevsky, L., Hollit, C., Maslennikov, V., Meffre, S., Gilbert, S., Bull, S., Scott, R., Emsbo, P., Thomas, H., 2009. Gold and trace element zonation in pyrite using a laser imaging technique: implications for the timing of gold in orogenic and carlin-style sediment-hosted deposits. Econ. Geol. 104, 635–668.

Lawley, C., Selby, D., Imber, J., 2013. Re-Os molybdenite, pyrite, and chalcopyrite geochronology, Lupa Goldfield, Southwestern Tanzania: tracing metallogenic time scales at midcrustal shear zones hosting orogenic Au deposits. Econ. Geol. 108, 1591–1613.

Li, G.S., Chen, J.R., Wang, Y.Z., Jin, B.Y., Wu, Y.H., Yu, W.Q., 2003. Study on the main mineralization type and the inclusion features of the Jinchang gold deposit, Heilongjiang. Gold Geol. 9, 32–37 (in Chinese with English abstract).
Li, J.W., Zhao, X.F., Zhou, M.F., Vasconcelos, P., Ma, C.Q., Deng, X.D., Souza, Z.S., Zhao, Y.X., Wu, G., 2008. Origin of the Tongshankou porphyry-skarn Cu–Mo deposit, eastern Yangtze craton, Eastern China: geochronological, geochemical and Sr–Nd–Hf isotopic constraints. Miner. Deposita 43, 315–336.
Liu, J., Wu, G., Li, Y., Zhu, M.T., Zhong, W., 2012. Re–Os sulfide (chalcopyrite, pyrite and molybdenite) systematics and fluid inclusion study of the Duobaoshan porphyry Cu (Mo) deposit, Heilongjiang Province, China. J. Asian Earth Sci. 49, 300–312.
Liu, S., Hu, R.Z., Gao, S., Feng, C.X., Feng, G.Y., Coulson, I.M., Li, C., Wang, T., Qi, Y.Q., 2010. Zircon U-Pb age and Sr-Nd-Hf isotope geochemistry of Permian granodiorite and associated gabbro in the Songliao Block, NE China and implications for growth of Juvenile crust. Lithos 114, 423–436.
Loftus-Hills, G., Solomon, M., 1967. Cobalt, nickel and selenium in sulphides as indicators of ore genesis. Miner. Deposita 2, 228–242.
Lu, Y.H., Zhang, Y., Lai, Y., Wang, Y.Z., 2009. LA-ICPMS zircon U-Pb dating of magmatism and mineralization in the Jinchang gold ore-field, Heilongjiang province. Acta Petrol. Sinica 25, 2902–2912 (in Chinese with English abstract).
Makoundi, C., Khin, Z., Large, R.R., Meffre, S., Lai, C.-K., Hoe, T.G., 2014. Geology, geochemistry and metallogenesis of the Selinsing gold deposit, central Malaysia. Gondwana Res. 26, 241–261.
Mao, J.W., Pirajno, F., Cook, N., 2011a. Mesozoic metallogeny in East China and corresponding geodynamic settings-an introduction to the special issue. Ore Geol. Rev. 43, 1–7.
Mao, J.W., Pirajno, F., Xiang, J.F., Gao, J.J., Ye, H.S., Li, Y.F., Guo, B.J., 2011b. Mesozoic molybdenum deposits in the East Qinling-Dabie Orogenic belt: characteristics and tectonic settings. Ore Geol. Rev. 43, 264–293.
Mao, J.W., Zhang, Z.C., Zhang, Z.H., Du, A.D., 1999. Re-Os isotopic dating of molybdenites in the Xiaoliugou W (Mo) deposit in the northern Qilian mountains and its geological significance. Geochim. Cosmochim. Acta 63, 1815–1818.
Mao, J., Pirajno, F., Lehmann, B., Luo, M., Berzina, A., 2014. Distribution of porphyry deposits in the Eurasian continent and their corresponding tectonic settings. J. Asian Earth Sci. 79, 576–584.
Maruyama, S., Santosh, M., Zhao, D., 2007. Superplume, supercontinent, and post-perovskite: Mantle dynamics and anti-plate tectonics on the Core-Mantle Boundary. Gondwana Res. 11, 7–37.
Mathur, R., Ruiz, J., Tornos, F., 1999. Age and sources of the ore at Tharsis and Rio Tinto, Iberian Pyrite Belt, from Re-Os isotopes. Miner. Deposita 34, 790–793.
Mathur, R., Ruiz, J., Munizaga, F., 2000a. Relationship between copper tonnage of Chilean base-metal porphyry deposits and Os isotope ratios. Geology 28, 555–558.
Mathur, R., Ruiz, J., Titley, S., Gibbins, S., Martogomo, W., 2000b. Different crustal sources for Au-rich and Au-poor ores of the Grasberg Cu-Au porphyry deposit. Earth Planet. Sci. Lett. 183, 7–14.
Mathur, R., Titley, S., Ruiz, J., Gibbins, S., Friehauf, K., 2005. A Re-Os isotope study of sedimentary rocks and copper-gold ores from the Ertsberg District, West Papua, Indonesia. Ore Geol. Rev. 26, 207–226.
Maydagán, L., Franchini, M., Lentz, D., Pons, J., McFarlane, C., 2013. Sulfide composition and isotopic signature of the Altar Cu-Au deposit, Argentina: constrains on the evolution of the porphyry-epithermal system. Canad. Mineral. 51, 813–840.
Maydagán, L., Franchini, M., Rusk, B., Lentz, D., Mcfarlane, C., Impiccini, A., Ríos, F.J., Rey, R., 2015. Porphyry to epithermal transition in the altar Cu-(Au-Mo) Deposit, Argentina, studied by cathodoluminescence, LA-ICP-MS, and fluid inclusion analysis. Econ. Geol. 110, 889–923.
Men, L.J., Sun, J.G., Zhao, J.K., Chen, L., Liang, S.N., Pang, W., Chen, D., 2008. Fluid inclusions in breccia-type copper-gold orebodies of Jinchang gold deposit, Dongning County, Heilongjiang Province. Miner. Deposits 27, 71–80 (in Chinese with English abstract).
Morelli, R.M., Creaser, R.A., Selby, D., Kelley, K.D., Leach, D.L., King, A.R., 2004. Re-Os sulfide geochronology of the Red Dog sediment-hosted Zn-Pb-Ag deposit, Brooks Range, Alaska. Econ. Geol. 99, 1569–1576.
Mu, T., Liu, G.G., Xu, K.C., 2000. The geological-geochemical characteristics and ore genesis of Jinchang gold deposit in Heilongjiang. Gold Geol. 6, 57–64 (in Chinese with English abstract).
Nie, F.J., Zhang, K., Liu, Y.F., Jiang, S.H., Liu, Y., Liu, Y., 2011. Indosinian magmatic activity and molybdenum, gold mineralization along the northern margin of North China Craton and adjacent area. J. Jilin Univ. (Earth Sci. Ed.) 41, 1651–1666 (in Chinese with English abstract).
Pirajno, F., Ernst, R.E., Borisenko, A.S., Fedoseev, G., Naumov, E.A., 2009. Intraplate magmatism in Central Asia and China and associated metallogeny. Ore Geol. Rev. 35, 114–136.
Qi, L., Gao, J.-F., Zhou, M.-F., Hu, J., 2013. The design of re-usable Carius tubes for the determination of rhenium, osmium and platinum-group elements in geological samples. Geostand. Geoanal. Res. 37, 345–351.
Qi, L., Zhou, M.-F., Gao, J., Zhao, Z., 2010. An improved Carius tube technique for determination of low concentrations of Re and Os in pyrites. J. Anal. At. Spectrom. 25, 585–589.
Qi, L., Zhou, M.-F., Wang, C.Y., Sun, M., 2007. Evaluation of a technique for determining Re and PGEs in geological samples by ICP-MS coupled with a modified Carius tube digestion. Geochem. J. 41, 407–414.
Qian, Y., Sun, F.Y., Li, B.L., Chen, J., Diwu, C.R., 2012. Geochemistry and U-Pb geochrony of zircon from granite porphyry of Jinchang gold deposit in Heilongjiang, China and its geological significance. J. Chengdu Univ. Technol. Sci. Technol. Ed. 39, 362–371 (in Chinese with English abstract).
Qing, M., Tang, M.G., Xiao, L., Zhao, Y.S., Han, X.J., 2012. Automatic Laser Probe $^{40}Ar/^{39}Ar$ isochron ages of the quatrz and sphalerite from the Jinchang gold deposit, Dongning County, Heilongjiang Province, and their prospecting implications. Geol. Prospect. 48, 991–999 (in Chinese with English abstract).
Redmond, P.B., Einaudi, M.T., Inan, E.E., Landtwing, M.R., Heinrich, C.A., 2004. Copper deposition by fluid cooling in intrusion-centered systems: new insights from the Bingham porphyry ore deposit, Utah. Geology 32, 217–220.
Ren, J.Y., Tamaki, K., Li, S.T., Zhang, J.X., 2002. Late Mesozoic and Cenozoic rifting and its dynamic setting in Eastern China and adjacent areas. Tectonophysics 344, 175–205.
Reich, M., Kesler, S.E., Utsunomiya, S., Palenik, C.S., Chryssoulis, S.L., Ewing, R.C., 2005. Solubility of gold in arsenian pyrite. Geochim. Cosmochim. Acta 69, 2781–2796.
Reich, M., Deditius, A., Chryssoulis, S., Li, J.-W., Ma, C.-Q., Parada, M.A., Barra, F., Mittermayr, F., 2013. Pyrite as a record of hydrothermal fluid evolution in a porphyry copper system: a SIMS/EMPA trace element study. Geochim. Cosmochim. Acta 104, 42–62.
Rudnick, R.L., Gao, S., 2003. Composition of the continental crust. In: Holland, H.D., Turekian, K.K. (Eds.), Treatise on Geochemistry. Elsevier-Pergaman, Oxford, pp. 1–64.
Safonova, I.Y., 2009. Intraplate magmatism and oceanic plate stratigraphy of the Paleo-Asian and Paleo-Pacific Oceans from 600 to 140 Ma. Ore Geol. Rev. 35, 137–154.
Schoenberg, R., Nagler, T.F., Kramers, J.D., 2000. Precise Os isotope ratio and Re-Os isotope dilution measurements down to the picogram level using multicollector inductively coupled plasma mass spectrometry. Int. J. Mass Spectrom. 197, 85–94.
Seedorff, E., Diles Jr., J.H., Proffett, J., Einaudi, M.T., Zurcher, L., Stavast, W.J.A., Johnson, D.A., Barton, M.D., 2005. Porphyry deposits: characteristics and origin of hypogene features. Economic Geology 100th Anniversary Volume 29, 251–298.
Selby, D., Kelley, K.D., Hitzman, M.W., Zieg, J., 2009. Re-Os sulfide (bornite, chalcopyrite and pyrite) systematics of the carbonate-hosted copper deposit at Ruby Creek, Southern Brooks Range, Alaska. Econ. Geol. 104, 437–444.
Sengör, A.M.C., Natal'in, B.A., Burtman, V.S., 1993. Evolution of the Altaid tectonic collage and Palaeozoic crustal growth in Eurasia. Nature 364, 299–307.
Shinohara, H., Hedenquist, J.W., 1997. Constraints on Magma Degassing beneath the Far Southeast Porphyry Cu–Au Deposit, Philippines. J. Petrol. 38, 1741–1752.
Stein, H.J., Morgan, J.W., Schersten, A., 2000. Re-Os dating of low-level highly radiogenic (LLHR) sulfides: the Harnas gold deposit, southwest Sweden, records continental-scale tectonic events. Econ. Geol. Bull. Soc. Econ. Geol. 95, 1657–1671.
Stein, H.J., Sundblad, K., Markey, R.J., Morgan, J.W., Motuza, G., 1998. Re-Os ages for Archean molybdenite and pyrite, Kuittila-Kivisuo, Finland and Proterozoic molybdenite, Kabeliai, Lithuania: testing the chronometer in a metamorphic and metasomatic setting. Miner. Deposita 33, 329–345.
Sillitoe, R.H., 2010. Porphyry copper systems. Econ. Geol. 105, 3–41.
Ulrich, T., Gunther, D., Heinrich, C.A., 2001. The evolution of a porphyry Cu-Au deposit, based on LA-ICP-MS analysis of fluid inclusions: Bajo de la Alumbrera, Argentina. Econ. Geol. 97, 1889–1920.
Walker, R.J., Morgan, J.W., 1989. Rhenium-osmium isotope systematics of carbonaceous chondrites. Science 243, 519–522.
Wang, F., Zhou, X.H., Zhang, L.C., Ying, J.F., Zhang, Y.T., Wu, F.Y., Zhu, R.X., 2006. Late Mesozoic volcanism in the Great Xing'an Range (NE China): timing and implications for the dynamic setting of NE Asia. Earth Planet. Sci. Lett. 251, 179–198.
Wang, K.Y., Qing, M., Zhang, X.N., Wan, D., Xiao, L., 2011. Study on the characteristics of fluid inclusions and metallogenic evolution of Jinchang gold deposit, Heilongjiang Province. Acta Petrol. Sinica 27, 1275–1286 (in Chinese with English abstract).
Wang, Y., Xi, B.B., Zhang, D.H., Zhang, W.H., 2007. Geochemical characteristics of fluid inclusions in Jinchang gold deposit, Heilongjiang Province. Miner. Deposits 26, 184–194 (in Chinese with English abstract).
Waters, P.J., Cooke, D.R., Gonzales, R.I., Phillips, D., 2011. Porphyry and epithermal deposits and $^{40}Ar/^{39}Ar$ geochronology of the Baguio district, Philippines. Econ. Geol. 106, 1335–1363.
Windley, B.F., Kröner, A., Guo, J.H., Qu, G.S., Li, Y.Y., Zhang, C., 2002. Neoproterozoic to Paleozoic Geology of the Altai Orogen, NW China: new zircon age data and tectonic evolution. J. Geol. 110, 719–737.
Wu, F.Y., Lin, J.Q., Wilde, S.A., Zhang, X.O., Yang, J.H., 2005. Nature and significance of the early Cretaceous giant igneous event in eastern China. Earth Planet. Sci. Lett. 233, 103–119.
Wu, F.Y., Sun, D.Y., Ge, W.C., Zhang, Y.B., Grant, M.L., Wilde, S.A., Jahn, B.M., 2011. Geochronology of the Phanerozoic granitoids in northeastern China. J. Asian Earth Sci. 41, 1–30.
Wu, H., Zhang, L., Pirajno, F., Shu, Q., Zhang, M., Zhu, M., Xiang, P., 2016. The Mesozoic Caosiyao giant porphyry Mo deposit in Inner Mongolia, North China and Paleo-Pacific subduction-related magmatism in the northern North China Craton. J. Asian Earth Sci. 127, 281–299.
Xiao, W.J., Han, C.M., Yuan, C., Sun, M., Lin, S.F., Chen, H.L., Li, Z.L., Li, J.L., Sun, S., 2008. Middle Cambrian to Permian subduction-related accretionary orogenesis of Northern Xinjiang, NW China: implications for the tectonic evolution of central Asia. J. Asian Earth Sci. 32, 102–117.

Xiao, W.J., Windley, B.F., Hao, J., Zhai, M.G., 2003. Accretion leading to collision and the Permian Solonker suture, Inner Mongolia, China: termination of the central Asian orogenic belt. Tectonics 22, 1–8.

Xu, W.L., Ji, W.Q., Pei, F.P., Meng, E., Yu, Y., Yang, D.B., Zhang, X.Z., 2009. Triassic volcanism in eastern Heilongjiang and Jilin provinces, NE China: chronology, geochemistry, and tectonic implications. J. Asian Earth Sci. 34, 392–402.

Yang, J.H., Wu, F.Y., Wilde, S.A., 2003. A review of the geodynamic setting of large-scale Late Mesozoic gold mineralization in the North China Craton: an association with lithospheric thinning. Ore Geol. Rev. 23, 125–152.

Yang, Z.F., Luo, Z.H., Lu, X.X., Cheng, L.L., Huang, F., 2011. Discussion on significance of Re content of molybdenite in tracing source of metallogenic materials. Miner. Deposits 30, 654–674 (in Chinese with English abstract).

Ying, L.J., Wang, C.H., Tang, J.X., Wang, D.H., Qu, W.J., Li, C., 2014. Re–Os systematics of sulfides (chalcopyrite, bornite, pyrite and pyrrhotite) from the Jiama Cu–Mo deposit of Tibet, China. J. Asian Earth Sci. 79, 497–506.

Zeng, Q., Liu, J., Qin, K., Fan, H., Chu, S., Wang, Y., Zhou, L., 2013. Types, characteristics, and time–space distribution of molybdenum deposits in China. Int. Geol. Rev. 55, 1311–1358.

Zeng, Q.-D., Sun, Y., Chu, S.-X., Duan, X.-X., Liu, J., 2015. Geochemistry and geochronology of the Dongshanwan porphyry Mo–W deposit, Northeast China: implications for the Late Jurassic tectonic setting. J. Asian Earth Sci. 97, 472–485.

Zhai, M.G., Zhu, R.X., Liu, J.M., Meng, Q.R., Hou, Q.L., Hu, S.B., Li, Z., Zhang, H.F., Liu, W., 2003. Time-range of Mesozoic tectonic regime inversion in eastern north China block. Sci. China (Ser. D) 33, 913–920 (in Chinese with English abstract).

Zhang, H.D., Zhang, H.F., Santosh, M., Li, S.R., 2014. Fluid inclusions from the Jinchang Cu–Au deposit, Heilongjiang Province, NE China: genetic style and magmatic-hydrothermal evolution. J. Asian Earth Sci. 82, 103–114.

Zhang, H.F., 2007. Wall-Rock Alteration, Mineralization Time and Deposite Type of the Jinchang Gold Deposit From Dongning, Heilongjiang Province, China. China University of Geosciences, Beijing (in Chinese with English abstract).

Zhang, H.F., Li, S.R., Santosh, M., Liu, J.J., Diwu, C.R., Zhang, H., 2013. Magmatism and metallogeny associated with mantle upwelling: Zircon U-Pb and Lu–Hf constraints from the gold-mineralized Jinchang granite, NE China. Ore Geol. Rev. 54, 138–156.

Zhang, L.C., Xiao, W.J., Qin, K.Z., Qu, W.J., Du, A.D., 2005. Re-Os isotopic dating of molybdenite and pyrite in the Baishan Mo-Re deposit, eastern Tianshan, NW China, and its geological significance. Miner. Deposita 39, 960–969.

Zhang, W.H., Qin, J.Y., Zhang, D.H., Tian, L., Wang, L.L., Wang, Y., 2008. Fluid inclusion indicators in prophyry Au deposits: taking Jinchang gold deposit, Heilongjiang Province as an example. Acta Petrol. Sinica 24, 2011–2016 (in Chinese with English abstract).

Zhao, Y.S., 2013. Porphyry Gold System of the Jinchang Camp in the Yanbian-Dongning Metallogenic Belt, NE China. China University of Geosciences, Beijing (in Chinese with English absract).

Zhao, Y.S., Yang, L.Q., Chen, Y.F., Qing, M., Yan, J.P., Ge, L.S., 2012. Geochemisry and zircon U-Pb geochronology of the diorite porphyry associated with the Jinchang Cu-Au deposit, Heilongjiang Province. Acta Petrol. Sinica 28, 451–467.

Zhou, J.B., Wilde, S.A., 2013. The crustal accretion history and tectonic evolution of the NE China segment of the Central Asian Orogenic Belt. Gondwana Res. 23, 1365–1377.

Zhou, T.H., Goldfarb, R.J., Phillips, N.G., 2002. Tectonics and distribution of gold deposits in China: an overview. Miner. Deposita 37, 249–282.

Zhu, C.W., Chen, J.R., Li, T.G., Cui, B., Jin, B.Y., Wang, K.Q., 2003. Geology and ore genesis of Jinchang gold deposit, Heilongjiang Province. Miner. Deposits 22, 56–64 (in Chinese with English abstract).

Zimmerman, A., Stein, H.J., Morgan, J.W., Markey, R.J., Watanabe, Y., 2014. Re-Os geochronology of the El Salvador porphyry Cu-Mo deposit, Chile: tracking analytical improvements in accuracy and precision over the past decade. Geochim. Cosmochim. Acta 131, 13–32.